DOI: https://doi.org/10.24425/amm.2026.1986

PIOTR MĄDRY[1*], PAULINA KOZERA[1], MICHAŁ MISIAK[1], KAMIL DYDEK[1], SZYMON DEMSKI[1], JAKUB KOTOWSKI[2], EVGENIA MADIA[3], PAWEŁ DURAŁEK[4], ANNA BOCZKOWSKA[1], MAIK GUDE[3]

# NANOCOMPOSITE SENSORS FOR MONITORING STRUCTURAL HEALTH IN POLYMER SANDWICH COMPOSITES

This preliminary study evaluated printed conductive meshes as embedded sensors for damage detection in polymer sandwich composites. Meshes based on thermoplastic polyurethane and thermoplastic copolyamide were placed in three positions. Electrical measurements were combined with impact testing, ultrasonic inspection, active thermography, and optical microscopy. Sensor response depended on mesh material and position. The thermoplastic polyurethane mesh was effective only at the core-laminate interface, whereas the copolyamide-based mesh showed thermal changes in all positions. Surface-mounted meshes produced the smallest delamination areas. The results confirm the potential of conductive printed meshes for thermographic damage detection in sandwich composites.

*Keywords:* Polymer sandwich composites; nanocomposite sensors; active thermography; carbon nanotubes; structural health monitoring

## 1. Introduction

Composite materials address the increasing demand of modern industry for lightweight, high-performance structural solutions by offering superior tensile strength, low thermal conductivity, and excellent corrosion resistance. These properties make them particularly suitable for applications in sectors such as aerospace and transportation. A key structural concept enabling such performance is sandwich architecture. In this configuration, the outer layers (facings) are manufactured from materials with high stiffness and strength, whereas the core is characterized by relatively low density. Consequently, the facings primarily sustain compressive and bending loads, while the core transfers shear stresses, resulting in an optimized strength-to-weight ratio of the overall structure [1,2]. However, the inherent multilayered architecture of sandwich composites also makes them susceptible to complex damage mechanisms, such as impact-induced delamination. This type of damage may facilitate moisture ingress and lead to progressive material degradation during service.

Conventional non-destructive testing (NDT) techniques, although effective, are often time-consuming, costly, and require temporary withdrawal of structures from operation. Therefore, increasing attention is being directed toward the development of smart structures equipped with integrated sensor networks, enabling continuous structural health monitoring (SHM). Such systems allow for real-time, accurate detection of damage without interrupting operational processes [3].

An example of such a multifunctional approach was reported by Pinto et al., who developed a smart composite material containing embedded shape memory alloy wires. In their work, the embedded conductive network was used not only for strain sensing through electrical resistance changes, but also as an internal Joule heating source for active thermographic damage visualization and de-icing. This study demonstrated that integrating functional conductive elements directly into the composite structure can reduce the need for external heating sources and enable in situ damage assessment [4].

Following this concept, significant advancements in sensing technologies have also been driven by the incorporation of nanomaterials, particularly carbon nanotubes (CNTs). Polymer-based nanocomposites incorporating CNTs exhibit enhanced electrical and thermal conductivity while maintain-

[1] WARSAW UNIVERSITY OF TECHNOLOGY, FACULTY OF MATERIALS SCIENCE AND ENGINEERING, WARSAW, POLAND
[2] AIR FORCE INSTITUTE OF TECHNOLOGY, WARSAW, POLAND
[3] DRESDEN UNIVERSITY OF TECHNOLOGY, INSTITUTE OF LIGHTWEIGHT ENGINEERING AND POLYMER TECHNOLOGY, DRESDEN, GERMANY
[4] TECHNOLOGY PARTNERS FOUNDATION, WARSAW, POLAND

* Corresponding author: piotr.madry.dokt@pw.edu.pl

ing favorable mechanical properties [3,5]. For instance, Park et al. demonstrated that the incorporation of CNTs into epoxy resins enables the detection of microcracks through monitoring electrical resistance variations under tensile loading [6]. Similarly, Thostenson and Chou employed high-shear mixing techniques to achieve uniform CNT dispersion, facilitating the formation of conductive networks with higher sensitivity to damage compared to conventional stiffness-based assessment methods [7]. Recent research has also focused on the development of CNT-based sensing networks directly integrated onto reinforcing fibers. Zhang et al. fabricated semiconductive glass fibers coated with multi-walled CNTs, enabling precise strain monitoring via resistance changes [8]. In a related approach, Rausch and Mäder developed polymer-CNT films deposited on fiber surfaces, demonstrating that sensor sensitivity can be effectively tuned by controlling CNT concentration and film thickness [9]. Despite these advances, most CNT-based sensing approaches rely on bulk dispersion or surface coating techniques, which often present challenges related to scalability, repeatability, and integration into practical composite structures. Moreover, such methods frequently require specially prepared laminates and strictly controlled laboratory conditions, limiting their applicability in industrial environments [10]. Alternative strategies include the use of discrete sensing elements such as CNT-based buckypaper membranes. Meng Wang et al. proposed the integration of such membranes on both sides of a composite laminate, demonstrating that electrical resistance monitoring enables the identification of microcrack initiation through characteristic resistance increases [6]. Furthermore, Jovarauskaite et al. showed that incorporating three-dimensional carbon fiber grids combined with CNT-modified epoxy matrices into sandwich composites allows for accurate detection and localization of damage, including indentation, puncture, and delamination. Their methodology, based on mapping local resistance variations and supported by finite element analysis of electric potential distribution, exhibited significantly enhanced sensitivity compared to unmodified laminates [7]. Recent developments in additive manufacturing have further expanded the potential of CNT-based composites. 3D printing technologies have enabled the fabrication of flexible and biocompatible sensing systems. Shar et al. developed a single-component CNT–silicone ink capable of producing high-resolution, self-supporting printed structures suitable for wearable sensors and heating elements [11]. However, these approaches are predominantly focused on soft elastomeric matrices and biomedical applications.

Although a wide range of SHM techniques has been investigated, including fiber Bragg grating (FBG) sensors [12], electrical impedance tomography [1], electromechanical impedance methods [1,13] and ultrasonic guided wave techniques [1,14] the integration of 3D-printed nanocomposite meshes directly into sandwich structures remains insufficiently explored and warrants further investigation.

In contrast, this work presents a preliminary investigation into the integration of 3D-printed CNT doped meshes into rigid sandwich-structured composites for structural health monitoring applications. Compared to previously reported techniques, 3D printing offers opportunities for scalable fabrication of reproducible sensor geometries, and as confirmed by the test results, the possibility of detecting defects resulting from the impact test using both ultrasonic testing and active thermography.

## 2. Materials

The subject of the study comprised sandwich structures fabricated using a honeycomb core and unidirectional glass fiber prepreg. Three-dimensional meshes, manufactured via additive manufacturing from filament doped with multi-walled carbon nanotubes (MWCNTs), were integrated into the laminate structure.

A unidirectional (UD) epoxy-glass fiber prepreg, HexPly® M9.6GF (Hexcel, Stamford, USA), was used for specimen fabrication. As the honeycomb core, HexWeb® HRH-10-3.2 (Hexcel, Stamford, USA) was employed.

Two conductive filaments were used for the fabrication of the meshes. The Ampere TPU filament (Print-Me, Gorzów Wielkopolski, Poland) is based on thermoplastic polyurethane (TPU). The second material was a filament based on thermoplastic copolyamide hot-melt adhesive (Vestamelt® 722, Evonik, Essen, Germany), modified with multi-walled carbon nanotubes (MWCNTs). The copolyamide-based material was prepared using a melt-blending approach, as described in [15], resulting in a conductive filament containing 10 wt.% of MWCNTs. Both materials exhibited electrical conductivity due to the presence of CNTs; however, they differed significantly in their mechanical and thermal behavior, as summarized in TABLE 1. In general, Vestamelt exhibits a higher elastic modulus, indicating increased stiffness, and a significantly lower elongation at break, suggesting limited plastic deformation and a tendency toward brittle-like behavior compared to TPU.

The meshes were fabricated using a Prusa MK4 3D printer (GLOBAL 3D, Nysa, Poland). All specimens had overall dimensions of 150×100 mm and exhibited a regular square pattern with an approximate cell size of 10×10 mm. Filaments were deposited sequentially in orthogonal directions (0°/90°), forming a grid

TABLE 1

Characteristics of used materials [15,16]

| | **Thermal properties** | **Elastic modulus** | **Tensile Strength** | **Elongation at break** |
|---|---|---|---|---|
| **Ampere TPU** | Softening: 138°C<br>Melting: 220°C | 0.15 GPa | 50 MPa | 450% |
| **Vestamelt® 722 (10 wt.% MWCNT)** | Melting: 107°C | 0.66 GPa | 30 MPa | 28,6% |

structure. The track width corresponded to the nozzle diameter (0.6 mm), and the total thickness resulted from two printed passes (TABLE 2). Visual inspection confirmed proper bonding at strand intersections. The sensor content was defined by the grid geometry rather than directly quantified as a volume fraction.

TABLE 2

Mesh 3D printing parameters

| Parameter | Fill | Nozzle diameter | Layer height | Print Speed | Number of Passes |
|---|---|---|---|---|---|
| Value | 15% | 0.6 mm | 0.2 mm | 35 mm/s | 2 |

For resistivity measurements, electrical connections between the printed meshes and the electrodes were established using copper tape. To ensure proper contact, a conductive epoxy resin containing silver particles was applied along the edges of the printed meshes. Subsequently, copper tape was attached in a double-sided configuration to encompass the sides of the printed meshes. Sandwich plates were manufactured using an autoclave curing process, incorporating the printed meshes. The preparation process is shown in Fig. 1.

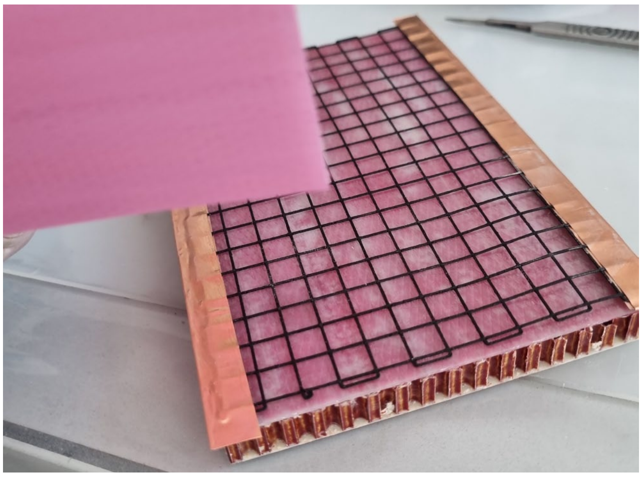

Fig. 1. Specimen preparation for the autoclave process

The plate dimensions were 100 mm×150 mm, in accordance with ASTM D7136 for composite materials subjected to low-velocity impact testing. Mesh was placed in three different positions within the composite structure: between the core and the first prepreg layer, between two prepreg layers, and on the sample surface. These configurations correspond to the KSPP, KPSP, and KPPS arrangements K – cellular core, S – 3D printed sensing mesh, P – prepreg layer as shown on Fig. 2.

The mesh and prepreg arrangement followed the configuration shown in TABLE 3, maintaining a consistent fiber orientation pattern: 0/90 – honeycomb core – 90/0, aligned with the sample's longer axis. In the specimen codes, the numerical prefix indicates the mesh material: 1 refers to Ampere TPU, whereas 2 refers to Vestamelt 722. The laminate was symmetrically reconstructed on both sides of the core. In this preliminary study, one specimen was fabricated and tested for each mesh material and sensor placement configuration, resulting in six sandwich plate systems in total. Autoclave curing was performed with a heating rate of 3°C/min up to 130°C, followed by a 3 h dwell at this temperature, in accordance with the prepreg manufacturer's recommended curing cycle.

TABLE 3

Fabricated sandwich plate systems

| Material type | Mesh | Mesh Placement in Laminate Layer | | |
|---|---|---|---|---|
| | | KSPP | KPSP | KPPS |
| Elastomer | Ampere TPU | 1KSPP | 1KPSP | 1KPPS |
| Thermoplastic Copolyamide | Vestamelt 722 | 2KSPP | 2KPSP | 2KPPS |

## 3. Methods

To assess the suitability of the filaments for sensor applications, their electrical conductivity was characterized. The electrical properties of the printed meshes were measured using a Keithley 6221/2182A source meter (Tektronix, Beaverton, Oregon, USA). Measurements were performed both prior to integration and after embedding the meshes into the composite, i.e. following the autoclave curing process. This approach enabled evaluation of the influence of the manufacturing process on the condition and performance of the sensors.

The purpose of the impact test was to introduce controlled damage into the structure to evaluate the effectiveness of the embedded sensing system. Impact testing was conducted using a specially designed experimental setup. The test involved the free fall of a mass of 5.526 kg, guided by a tubular fixture with a diameter larger than that of the impactor, ensuring controlled vertical motion. The impact energy was set to 30 J. The experiments were performed in accordance with ASTM D7136.

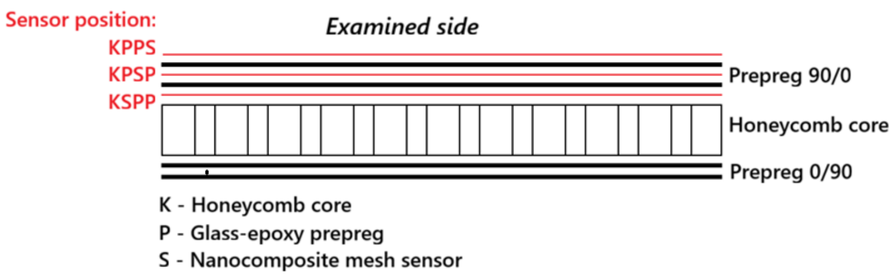


Fig. 2. Scheme of specimen structure and sensor placement configurations

To determine the occurrence and extent of damage resulting from the impact test, ultrasonic C-scan inspection was performed using a Dolphicam 2 portable device (Dolphitech AS, Oslo, Norway) operating at 5 MHz. During the examination, AMP (amplitude) analysis was applied based on mapping of the reflected ultrasonic signal, which enabled clear visualization of the internal structure and impact-induced defects such as delamination. The measurements were carried out both before and after impact in order to overlay the images and isolate the actual delaminated area. The processed images were then analyzed using ImageJ software, which allowed accurate determination of the delamination surface area.

Active thermography was performed to evaluate the ability of the embedded mesh structures to act as thermal energy sources and to determine whether impact-induced damage could be identified based on changes in their heating behavior. The specimens were heated by Joule heating generated by electrical current flowing through the integrated meshes, and infrared images were acquired using a FLIR SC7000 thermal imaging system (FLIR LLC, Wilsonville, Oregon, U.S.). Thermographic measurements were conducted both before and after impact testing in order to characterize the heating performance of the meshes and to assess possible alterations in temperature distribution in the vicinity of the damaged zone. The camera operated at 10 frames per second (10 fps), which enabled analysis of temperature-time profiles at selected surface locations on each specimen.

Light microscopy was used to visualize the type of damage to the sample and sensor. The examination was performed using a Keyence VHX-7000 light microscope (KEYENCE, Mechelen, Belgium) with a magnification of up to 250×.

## 4. Results and discussion

### 4.1. Filament electrical conductivity and sensor resistance results

Both filaments exhibited conductive behavior, indicating the formation of a continuous conductive network within the polymer matrix. However, the TPU-based filament showed approximately fourfold higher electrical conductivity than the Vestamelt 722-based material. It should be noted that the conductivity of the raw filament does not directly correspond to the electrical response of the printed mesh, which is additionally affected by mesh geometry and inter-path contact resistance. As shown in TABLE 4, the coPA-based meshes exhibited lower resistance before implementation, while after processing a significant increase in resistance was observed for the KSPP configuration in both material systems. This effect is likely related to the position of the mesh between the prepreg layer and the honeycomb core, where localized pressure from the cell walls and lack of support over the cell openings could promote deformation and partial disruption of conductive paths. In contrast, the surface-mounted meshes retained the lowest resistance after implementation, suggesting that this configuration was least affected by the composite manufacturing process.

TABLE 4

Filament electrical conductivity and mesh resistance before and after implementation

| Filament | σ [S/m] | Mesh | Resistance [kΩ] | |
|---|---|---|---|---|
| | | | Before implementation | Post implementation |
| Ampere TPU | 13.5±0.25 | 1KSPP | 6.38±0.79 | 45.27 |
| | | 1KPSP | | 174.8 |
| | | 1KPPS | | 1.64 |
| Vestamelt 722 | 3.38±1.07 | 2KSPP | 0.93±0.16 | 14.7 |
| | | 2KPSP | | 1.62 |
| | | 2KPPS | | 1.97 |

### 4.2. Ultrasonic testing result

The results indicate that all samples exhibited visible structural changes as a result of impact. The extent of damage varied between samples, and a representative example of a sample before and after impact is shown in Fig. 3.

Quantitative measurements of the delaminated area clearly confirmed differences between the tested configurations. For both materials, the specimens with the mesh located on the surface exhibited the smallest delamination areas. Detailed results are summarized in TABLE 5. At the same time, the influence of mesh material was less consistent than the effect of mesh location.

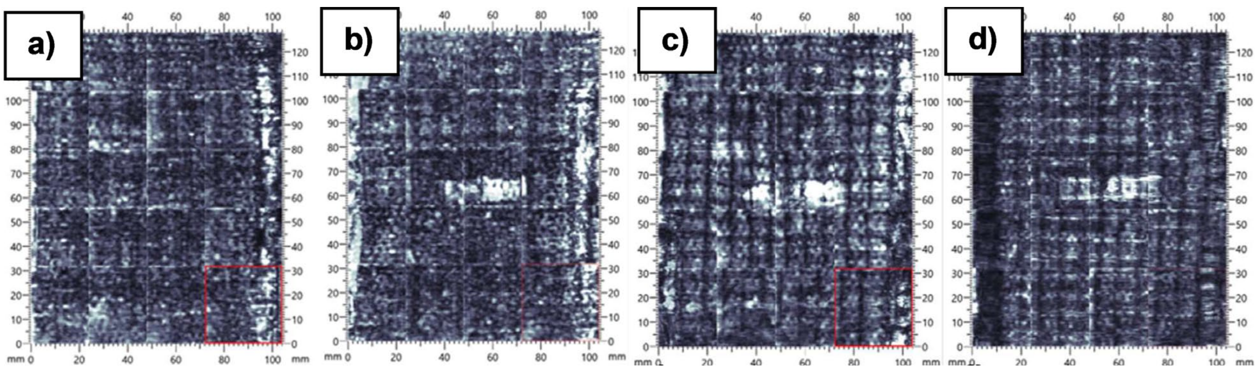


Fig. 3. C-scan analysis of samples in AMP mode: a) 1KSPP before impact, b) 1KSPP after impact, c) 1KPSP after impact, d) 1KPPS after impact

TABLE 5

Delamination area determined by ultrasonic C-scan analysis

| Filament | Sample-Mesh | Delamination area [mm$^2$] |
|---|---|---|
| **Ampere TPU** | 1KSPP | 151 |
| | 1KPSP | 249 |
| | 1KPPS | 92 |
| **Vestamelt 722** | 2KSPP | 172 |
| | 2KPSP | 114 |
| | 2KPPS | 84 |

The smaller delamination areas observed for surface-mounted meshes may be explained by the fact that this configuration does not directly interfere with the internal laminate architecture or the bonding region between the honeycomb core and the prepreg layers. As a result, its influence on interlaminar integrity is expected to be limited.

### 4.3. Thermographic test results

Thermograms recorded before and after impact, together with temperature-time curves obtained for selected points, were used to evaluate the heating behavior of the specimens and the influence of damage on their thermal response. A representative set of thermograms and corresponding heating curves is shown in Fig. 4. For each specimen, at least one observation point was selected within the impact zone and one in the area reaching the highest temperature.

The heating uniformity and heating time differed between the tested configurations. From the sensor performance perspective, the desired response was assumed to involve relatively fast and uniform heating of the specimen surface. However, the most important parameter was the change in heating behavior in the impact zone. The detailed quantitative results are summarized in TABLE 6. The heating rate also appeared to be closely related to the electrical resistance of the embedded meshes. In general, lower mesh resistance was associated with faster heating of the specimen, whereas the 1KPSP configuration, which exhibited the highest resistance after implementation (174.8 kΩ), showed clearly reduced heating efficiency. In this case, despite the longest current application time, the maximum recorded temperature reached only 32°C.

The results show that the thermal response of the hottest regions, treated as reference points, changed only slightly after impact. In some cases, including 1KPSP, 1KPPS and 2KPPS, a decrease in maximum temperature was observed, whereas for 2KPSP a local increase was recorded. Such fluctuations may result from redistribution of current within the conductive network

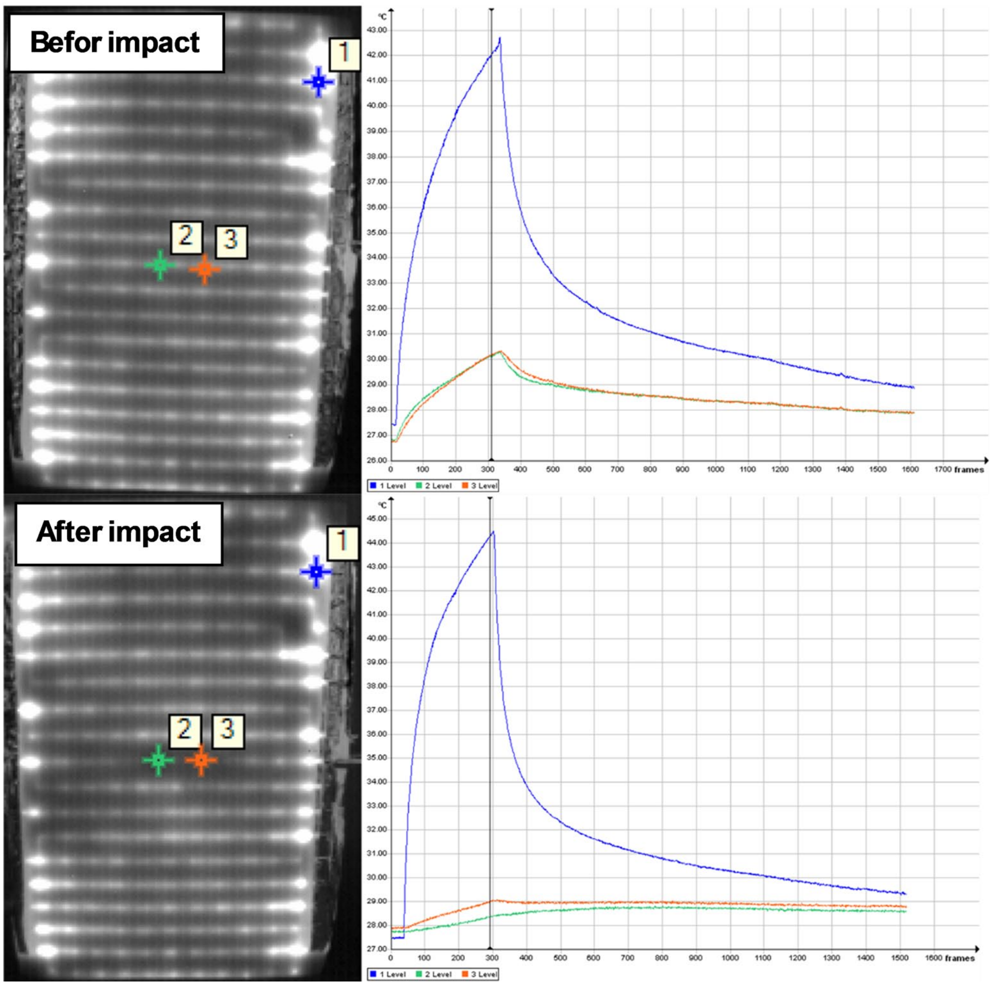


Fig. 4. Thermographic results obtained for specimen 2KPSP before and after impact

TABLE 6

Thermographic results before and after impact. $T_{max}$ – maximum temperature; $T_i$ – temperature in the impact zone

| Sample | Heating time [s] | Before impact | | After impact | | | |
|---|---|---|---|---|---|---|---|
| | | $T_{max}$ [°C] | $T_i$ [°C] | $T_{max}$ [°C] | $\Delta T_{max}$ | $T_i$ [°C] | $\Delta T_i$ |
| **1KSPP** | 25 | 42.0 | 32.4 | 41.8 | – | 28.0 | ↓ |
| **1KPSP** | 110 | 32.7 | 26.5 | 31.0 | ↓ | 26.5 | – |
| **1KPPS** | 70 | 41.0 | 38.7 | 39.0 | ↓ | 38.0 | ↓ |
| **2KSPP** | 40 | 35.3 | 31.2 | 35.0 | – | 27.6 | ↓ |
| **2KPSP** | 30 | 42.0 | 30.0 | 44.0 | ↑ | 28.2 | ↓ |
| **2KPPS** | 30 | 37.5 | 31.7 | 32.3 | ↓ | 27.5 | ↓ |

Note: "–" no significant change; "↓" decrease after impact, "↑" increase after impact.

after partial damage, causing other regions of the mesh to carry a larger portion of the electrical load. More importantly, a temperature decrease in the impact zone was observed in five out of six specimens. This behavior may indicate local disruption of the conductive path and is therefore consistent with the expected sensor response. However, the practical effectiveness of the sensor ultimately depends on whether the damage can also be identified directly from the thermograms. Therefore, Fig. 5 presents thermograms of all specimens recorded before and after impact.

A comparison of the thermograms before and after impact further confirmed that the damage-related change in heating behavior depended on both mesh material and its location within the laminate. For the TPU-based meshes, only the KSPP configuration provided a sufficiently clear thermal indication of damage. In contrast, the Vestamelt 722-based meshes showed visually apparent changes in heating behavior in all tested configurations, while the temperature-time curves additionally confirmed these differences. The 1KPPS specimen did not allow reliable identification of damage based on direct thermogram comparison, and although a temperature decrease was observed in the impact zone, it was proportional to the decrease recorded in the hottest region. Therefore, this case was not considered as clear indication of impact-induced sensor response.

### 4.4. Microstructure analysis using light microscopy

Optical microscopy of cross-sections taken from the impact zone was performed to assess the degradation of the embedded meshes and to determine whether their presence could affect damage development in the composite structure. The observed failure modes in the sandwich specimens included interlaminar delamination, through-thickness cracking of the laminate, and local crushing of the honeycomb core. In the meshes, the dominant damage mechanisms were debonding from the surrounding matrix and local fracture or fragmentation of the printed structure. Representative examples are shown in Fig. 6.

The observations indicate that mesh location had a major influence on the damage mechanism. In the KPSP configuration, the mesh was consistently located at the delamination boundary, which may suggest that it acted as a local interfacial discontinuity promoting interlaminar damage initiation. In the KSPP configuration, the meshes exhibited clear waviness and out-of-plane distortion, consistent with the previously proposed mechanism related to localized pressure from the honeycomb cell walls and lack of support over the cell openings. This behavior is also consistent with the increased electrical resistance observed for this configuration. In the KSPP arrangement, the mesh

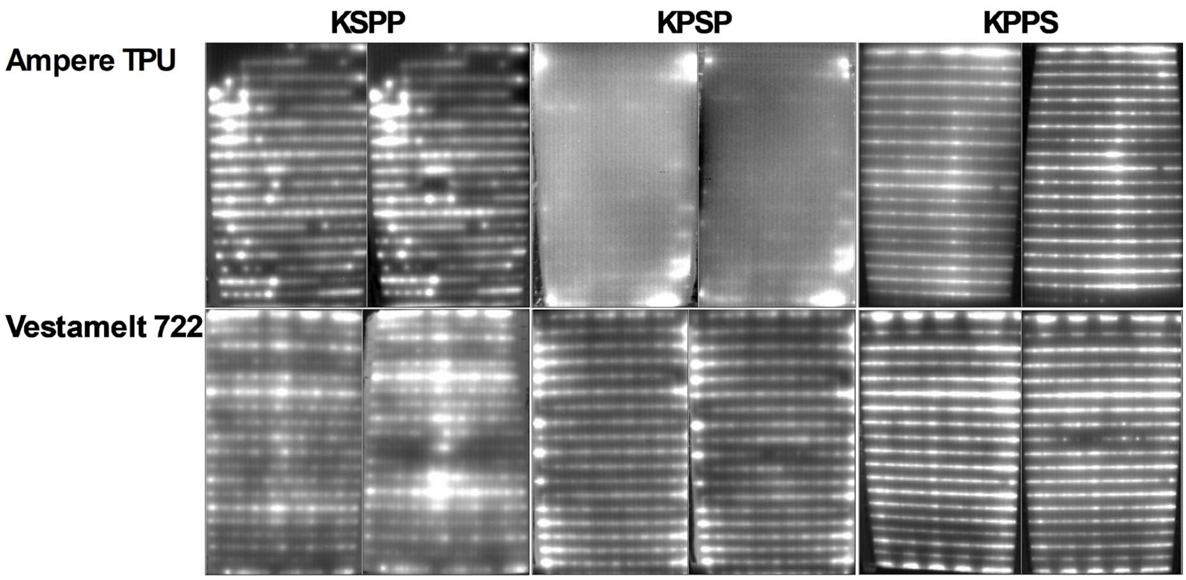


Fig. 5. Thermograms of all tested specimens before and after impact. For each configuration, the pre-impact image is shown on the left and the post-impact image on the right

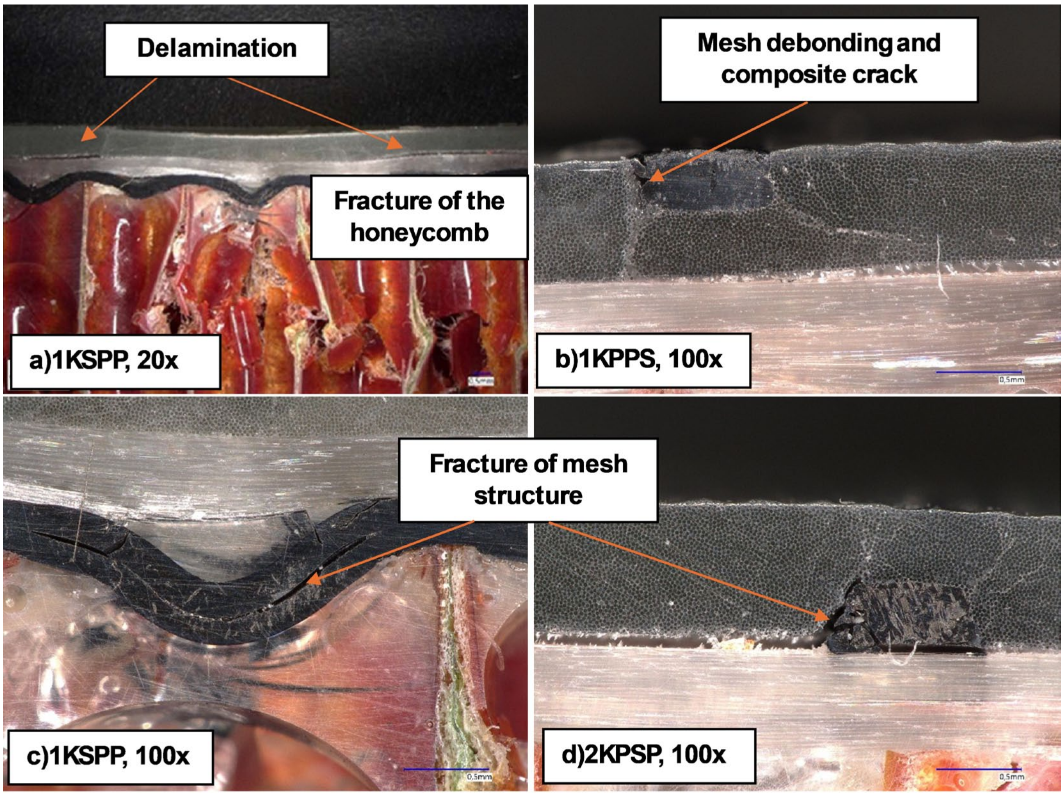


Fig. 6. Representative light microscopy images of structural defects observed after impact

experienced non-uniform deformation during manufacturing, being locally compressed at the honeycomb walls and deflected in the unsupported regions above the cell openings. Microscopy revealed both local crushing of mesh fragments supported by the honeycomb and separation of printed paths in the waved, unsupported regions. Owing to its high flexibility, the Ampere TPU mesh did not fracture readily under deformation alone; however, the pre-stressed state introduced by this configuration likely made it more susceptible to impact-induced disruption. This interpretation is supported by the thermographic results, as KSPP was the only TPU-based configuration that showed a clear damage-related change in heating behavior.

More pronounced material-related differences were observed for the surface-mounted meshes. In the case of Ampere TPU, only minor interfacial debonding was observed, while the internal continuity of the mesh remained largely preserved. In contrast, the Vestamelt 722-based meshes tended to fracture as a continuation of the laminate crack path. This may indicate that the interfacial adhesion in this case exceeded the cohesive strength of the mesh material itself. Such behavior is consistent with the difference in deformability of the two materials: the elastomeric TPU is more likely to undergo debonding while maintaining structural continuity, whereas the stiffer copolyamide-based material is more prone to fracture under local stress. This difference was also reflected in the thermographic response: the KPPS configuration based on Vestamelt 722 showed a visible change in heating behavior after impact, whereas no comparable thermographic contrast was observed for the more deformable Ampere TPU in the same configuration.

## 5. Conclusions

The performed study showed that the sensing performance of 3D-printed conductive meshes embedded in sandwich composites depended strongly on both the material of the mesh and its position within the structure. Based on microscopic observations, the Ampere TPU mesh behaved as an elastomeric material and did not fracture sufficiently to provide an effective sensing response in the KPSP and KPPS configurations. A distinct damage-related response was obtained only in the KSPP configuration, where the non-uniform loading imposed by the honeycomb core introduced additional local stresses into the mesh. As a result, impact loading led to disruption of the printed paths, which was reflected in the thermographic response.

A different behavior was observed for the Vestamelt 722-based meshes, which showed changes in heating behavior for all tested positions. This suggests that the bonding between the mesh and the surrounding composite was strong enough for crack propagation in the composite to be transferred into the mesh structure, instead of causing simple interfacial debonding, as observed for Ampere TPU.

Mesh location also had a strong influence on electrical resistance after implementation. Meshes placed at the honeycomb interface became locally bent and distorted, which increased the resistance of the conductive paths. In contrast, surface-mounted meshes, supported by a flat tool surface and uniformly pressed by the prepreg, retained much lower resistance. This was later reflected in the heating efficiency: specimens with mesh resistance of about 2 kΩ heated rapidly and effectively, whereas the 1KPSP specimen, characterized by the highest resistance (174.8 kΩ), did not allow efficient heating of the structure.

Another important aspect was the influence of the mesh on the structural integrity of the monitored composite. In this respect, the KPPS configuration was the most favorable, since the smallest delamination areas were observed for both materials when the mesh was placed on the laminate surface. Overall, the results indicate that Vestamelt 722 shows particularly promising potential as a sensing material for this type of application, while surface placement appears to be the most beneficial solution when minimizing structural damage is a priority.

From a practical perspective, the proposed approach may reduce the need for complete withdrawal of the monitored structure from service and shorten inspection time by enabling local damage indication through direct visualization of changes in the heating pattern. Compared with conventional active thermography, where external lamps or heaters are required to uniformly excite the inspected surface, the use of an embedded conductive mesh provides an internal heat source, which may be particularly advantageous for large or difficult-to-access structures.

Although the present study is preliminary, it confirms that 3D-printed meshes based on filaments modified with conductive nanotubes have clear potential for thermographic damage detection in sandwich composites and provide a basis for further research in this field.

**Acknowledgements**

This research was conducted within the COMP-ECO project (Strengthening Mazovian multifunctional composite ecosystem through holistic approach and strategic alliance with European leaders), funded by the Horizon Europe Framework Programme (Grant Agreement No. 101079250).

## REFERENCES

[1] C. Kralovec, M. Schagerl, Review of Structural Health Monitoring Methods Regarding a Multi-Sensor Approach for Damage Assessment of Metal and Composite Structures. Sensors **20** (3), 826 (2020). DOI: https://doi.org/10.3390/s20030826

[2] A. Boczkowska, J. Kapuściński, Z. Lindemann, D. Witemberg-Perzyk, S. Wojciechowski, Kompozyty, Oficyna Wydawnicza Politechniki Warszawskiej, Warszawa (2003).

[3] A. Kausar, I. Ahmad, Highpoints of carbon nanotube nanocomposite sensors – A review. E-Prime – Adv. Electr. Eng. Electron. Energy **7**, 100419 (2024). DOI: https://doi.org/10.1016/j.prime.2024.100419

[4] F. Pinto, F. Ciampa, M. Meo, U. Polimeno, Multifunctional SMArt composite material for in situ NDT/SHM and de-icing. Smart Mater. Struct. **21** (10), 105010 (2012). DOI: https://doi.org/10.1088/0964-1726/21/10/105010

[5] M. Wang, N. Li, G.-D. Wang, S.W. Lu, Q.D. Zhao, X.L. Liu, High-sensitive flexural sensors for health monitoring of composite materials using embedded carbon nanotube (CNT) buckypaper. Compos. Struct. **261**, 113280 (2021). DOI: https://doi.org/10.1016/j.compstruct.2020.113280

[6] J.-M. Park, D.-S. Kim, S.-J. Kim, P.-G. Kim, D.-J. Yoon, Inherent sensing and interfacial evaluation of carbon nanofiber and nanotube/epoxy composites using electrical resistance measurement and micromechanical technique. Compos. Part B Eng. **38** (7), 847-861 (2007). DOI: https://doi.org/10.1016/j.compositesb.2006.12.004

[7] E.T. Thostenson, T.-W. Chou, Carbon nanotube networks: sensing of distributed strain and damage for life prediction and self-healing. Adv. Mater. **18** (21), 2837-2841 (2006). DOI: https://doi.org/10.1002/adma.200600977

[8] H. Zhang, E. Bilotti, T. Peijs, The use of carbon nanotubes for damage sensing and structural health monitoring in laminated composites: a review. Nanocomposites **1** (4), 177-194 (2016). DOI: https://doi.org/10.1080/20550324.2015.1113639

[9] J. Rausch, E. Mäder, Health monitoring in continuous glass fibre reinforced thermoplastics: manufacturing and application of interphase sensors based on carbon nanotubes. Compos. Sci. Technol. **70** (11), 1589-1596 (2010). DOI: https://doi.org/10.1016/j.compscitech.2010.05.018

[10] L. Gao, T.-W. Chou, E.T. Thostenson, Z. Zhang, A comparative study of damage sensing in fiber composites using uniformly and non-uniformly dispersed carbon nanotubes. Carbon **48** (13), 3788-3794 (2010). DOI: https://doi.org/10.1016/j.carbon.2010.06.041

[11] A. Shar, P. Glass, S.H. Park, D. Joung, 3D printable one-part carbon nanotube–elastomer ink for health monitoring applications. Adv. Funct. Mater. **33**, 2211079 (2023). DOI: https://doi.org/10.1002/adfm.202211079

[12] R. Di Sante, Fibre optic sensors for structural health monitoring of aircraft composite structures: recent advances and applications. Sensors **15** (8), 18666-18713 (2015). DOI: https://doi.org/10.3390/s150818666

[13] V. Giurgiutiu, Structural Health Monitoring with Piezoelectric Wafer Active Sensors. Academic Press, Cambridge (2014).

[14] Z. Yang, H. Yang, T. Tian, D. Deng, M. Hu, J. Ma, D. Gao, J. Zhang, S. Ma, L. Yang, H. Xu, Z. Wu, A review on guided-ultrasonic-wave-based structural health monitoring: from fundamental theory to machine learning techniques. Ultrasonics **133**, 107014 (2023). DOI: https://doi.org/10.1016/j.ultras.2023.107014

[15] P. Latko-Durałek, M. Misiak, A. Boczkowska, Electrically conductive adhesive based on thermoplastic hot melt copolyamide and multi-walled carbon nanotubes. Polymers **14** (22), 4371 (2022). DOI: https://doi.org/10.3390/polym14224371

[16] dddrop, Datasheet TPU, accessed: 24.04.2026 available at: https://pdf.directindustry.com/pdf/dddrop/datasheet-tpu/198634-770640.html